AUT Journal of Mechanical Engineering

AUT J. Mech. Eng., 6(2) (2022) 217-228
DOI: 10.22060/ajme.2022.20395.6000

Effects of Shape Memory Alloys and Carbon Nanotubes on the Nonlinear Aerothermal Flutter Characteristics of Hybrid Nanocomposite Beam

H. Heidari*, S. Esmaeili, A. Hakimi

Department of Mechanical Engineering, Malayer University, Malayer, Iran

ABSTRACT: In this study, the effect of aerodynamic and thermal forces on the flutter stability of an epoxy / fiber-based hybrid nanocomposite beam containing shape memory alloy wires and reinforced by functionally graduated distribution of carbon nanotubes are investigated. Carbon nanotubes help to increase the stiffness of the nanocomposite beam, and the shape memory alloys will increase the flutter stability boundaries by inducing tensile stress in the beam due to the increase in temperature and the aerodynamic pressure. In this study, the Brinson model is supposed to present the properties of shape memory alloy wires, also, the Euler-Bernoulli beam model is assumed to be in line with van-Karmen nonlinear strains. The boundaries of buckling stability and aerothermodynamics flutter have been investigated by studying the natural frequencies of the hybrid nanocomposite beam and the thermal bifurcation points. The primary objective of this study is to examine the impact of carbon nanotubes and shape memory alloy wire on improving the behavior of a composite beam flutter under the effect of airflow and temperature increase, simultaneously. The results showed that applying these two advanced reinforcing materials has a significant impact on increasing the static and dynamic stabilities of hybrid nanocomposite beams in the thermo-aerodynamic environment.

Review History:

Received: Aug. 12, 2021
Revised: Nov. 05, 2021
Accepted: Dec. 21, 2021
Available Online: Jan. 07, 2022

Keywords:

Shape memory alloy
Carbon nanotube reinforcement
Hybrid nanocomposite beam
Nonlinear equation
Aerothermal flutter

1- Introduction

The application of smart materials in engineering and sciences has attracted the attention of scientists to study the behaviors of these structures at different loading conditions. Shape Memory Alloys (SMAs), which are classified as intelligent materials, have unique behaviors such as the capability to deform and recover the original shape at the combination of mechanical and thermal loads. The specific properties of SMAs could be used in various industrial sectors such as aerospace, automotive, and biomechanics [1].

Feng and Li [2] numerically and experimentally studied the dynamic behavior of a discrete mechanical system involving mass, damper, and a rod element made of SMAs. The effect of phase change on the resonant frequency and the maximum response near the resonant frequency was investigated. Bernardini and Rega [3] investigated the chaotic behavior of a single degree of freedom system consisting of a memory alloy rod element. They studied the influence of temperature, heat transfer rate, and thermal capacity on the chaotic behavior of the system. Savi and Paco [4] and Machado et al. [5] examined the forced and free vibrations of a two-degree-of-freedom coupling system consisting of SMA elements in terms of chaotic behaviors and damping effects. Using numerical and experimental analysis, Lagodas et al. [6] investigated the damping vibration of the mechanical system whose main element was a memory alloy wire. Frequency response and deformability of memory wire and the temperature changes during the test were considered.

The dynamic stability of a composite beam reinforced with memory alloy wires was investigated by Tsai and Chen [7]. In their research, the composite beam was affected by the axial force and the instability range of the composite was identified using the finite element method along with the harmonic balance method. Khalili et al. [8] investigated the energy dissipation effects of embedded wires in the upper and lower surfaces of a composite beam .Hashemi and Khadem [9] studied the vibrational behavior of a cantilever beam made of shape memory alloy. The beam is simplified as a discrete mass and spring system, and the vibration behavior of the beam for the quasi-elastic working range was investigated. Daman Pak et al. [10] analyzed the vibration behavior of two-and three-layer beam containing SMAs using a numerical method taking into account the influence of prestressing temperature and beam thickness. Samadpour et al. [11] considered the nonlinear vibration and thermal post-buckling analysis of composite beams reinforced by memory alloy fibers with symmetrical and asymmetrical layers, using the Euler-Bernoulli theory and Brinson model. Also, Asadi and Beheshti [12] investigated the free vibration of composite beams reinforced by SMA wires using Timoshenko's theory and the Brinson model.

Samadpour et al. [11], studied the nonlinear flutter and

*Corresponding author's email: hr.heidadri@malayeru.ac.ir

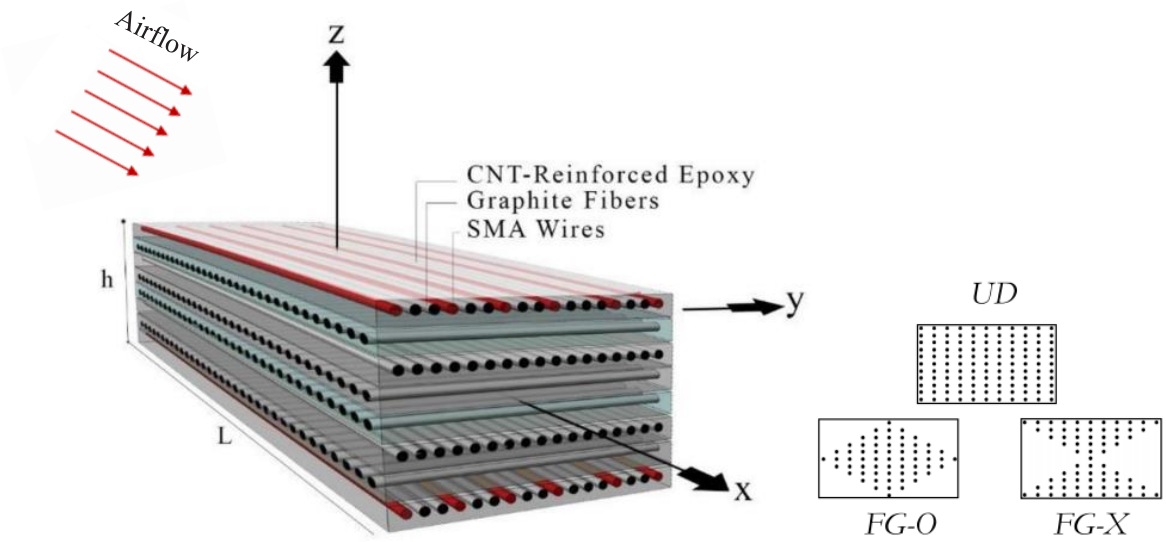

Fig. 1. Schematic of a hybrid composite beam containing SMA / CNT with three distributions of CNTs and airflow

thermal buckling response of a fiber-reinforced composite beam with memory alloy wires under simultaneous thermal and aerodynamic loading using the Galerkin method. They examined the influence of memory alloy wires on improving the flutter's behavior of composite beams at supersonic speeds. Asadi and Beheshti [12] investigated numerically the aerothermodynamics response of Carbon Nanotube (CNT) reinforced beams under ultrasonic airflow in a thermal environment using first-order shear deformation theory and third-order piston theory at different boundary conditions. Lin et al. [13] presented a nonlinear analytical model to investigate the aeroacoustics flutter and the response of composite panels with memory alloy wires to random excitation using the third-order shear deformation theory. Rostami et al. [14], studied the thermal buckling and post-buckling of sheets containing memory wires considering nonlinear strains using the semi-analytical method.

In recent years, Carbon Nanotubes Reinforced Composite Structures (CNTRCs) have had extensive applications in various industries and engineering fields due to their extraordinary mechanical strength/stiffness features [15]. The existence of CNTRCs improves the strength and stability of the structure due to its better mechanical and chemical properties [16], which inspire scientists to emphasize supplementary the study of deformation, vibration, and buckling of these structures. Thanks to the outstanding properties of CNTRCs and specific properties of SMA materials, the hybrid nanocomposite structures with integrated SMA wires offer great potential for use in engineering, advanced aerospace, military, and automotive structural applications. These structures are applied as smart structures to control the free vibration, suppress the forced vibration and decrease the deflection, delay the buckling, decrease the post-buckling deflection, and flutter control. These composite structures are frequently subjected to large thermal gradients while being exposed to the actual environments like the aerodynamic pressure or solar radiations [17].

Natural frequency analysis of the CNT-reinforced composite structure embedded with SMA fiber has been considered numerically via a micromechanical multiscale FE material model by Mehar et al. [18]. The multiscale, multi-fiber-reinforced (SMA/CNT) polymeric composite was under the elevated thermal environment. Also, Mehar et al. [19] have made an effort to predict the thermal buckling load parameter of nanotube-reinforced hybrid composite shell panel embedded with SMA fiber through a higher-order isoperimetric Finite Element (FE) technique. They showed the thermal stability of the hybrid (SMA/CNT/polymer) composite is increasing with higher volume fractions of CNT and SMA. As observed above, in all mentioned literatures no investigation has been carried out on the simultaneous effect of SMA fibers and carbon nanotubes on flutter suppression and the analysis of nonlinear aerothermal flutter characteristics of hybrid nanocomposite beam

In this study, a novel graded hybrid reinforcement is proposed for a nanocomposite beam. Both reinforcing materials, SMA wires, and CNTs are used in the structure to create a hybrid composite with new material properties. The novelties can be declared as presenting a new composite design for developing the modeling for the aerothermodynamics flutter behavior of a hybrid nanocomposite beam. The main objective is to simultaneously examine the impact of CNTs and alloy memory wire on improving the behavior of composite beam flutter under the effect of ultrasonic flow and significant heat increase.

2- Mathematical Modeling and Equilibrium Equations

2- 1- Hybrid nanocomposite properties

Consider a laminated composite beam, as shown in Fig. 1. The beam is made of epoxy and long graphite fibers and is assumed to be in a thermal environment with uniform temperature.

Table 1. Material properties of epoxy [20]

Property	Value
Young modulus	3.1 GPa
Poisson ratio	0.35
Glass transition temperature	112.5 ^{0}C
Coefficient of Thermal Expansion (CTE)	66×10^{-6} 1/^{0}C

In the present study, the first two tactics (using SMA wires and CNTs) are examined. In the first step, shape memory wires are embedded in the composite medium to produce tensile recovery stress in the structure. Then, CNTs are added to the epoxy to form a new polymer matrix with better material properties. Finally, both reinforcing materials, SMA wires, and CNTs, are used in the structure to create a hybrid composite with new material properties and tensile recovery stress as follows:

$$\{\sigma\}=[Q]_{new}\left(\{\varepsilon\}-\Delta T\{\alpha\}_{new}\right)+\left\{\sigma^{tensile}\right\} \quad (1)$$

Table 1 shows the thermo-mechanical properties of epoxy LY5052 applied in the present work.

Therefore, using the micro-mechanical model [21] in Eq. (2), the thermo-mechanical characteristics of the graphite fiber/epoxy composite beam can be calculated.

$$\begin{aligned}
&E_{11}=E_fV_f+E_m\left(1-V_f\right);\\
&E_{22}=E_m\left[\left(1-\sqrt{V_f}\right)+\frac{\sqrt{V_f}}{1-\sqrt{V_f}\left(1-\frac{E_m}{E_{2f}}\right)}\right]\\
&G_{12}=G_{13}=G_m\left[\left(1-\sqrt{V_f}\right)+\frac{\sqrt{V_f}}{1-\sqrt{V_f}\left(1-\frac{G_m}{G_{12f}}\right)}\right]\\
&\alpha_1=\frac{V_f\alpha_fE_f+\left(1-V_f\right)\alpha_mE_m}{E_{11}}\\
&\alpha_2=\frac{E_m}{E_{22}}\left[\alpha_m\left(1-\sqrt{V_f}\right)+\frac{\alpha_m\sqrt{V_f}-V_f\left(\alpha_m-\alpha_{2f}\right)}{1-\sqrt{V_f}\left(1-\frac{E_m}{E_{2f}}\right)}\right]\\
&\nu_{12}=\nu_{12f}V_f+\nu_{12m}\left(1-V_f\right)\\
&\rho=\rho_fV_f+\rho_m\left(1-V_f\right);
\end{aligned} \quad (2)$$

In which the subscripts m and f mean the matrix and fiber, respectively. Also, parameters E, G, α, ρ and V_f denote young modulus, shear modulus, Poisson ratio, thermal expansion coefficient, material density, and volume fraction of fibers, respectively

The material properties of long graphite fibers are provided in Table 2. It should be mentioned that the volume fraction of long fibers is assumed to be 55% in the present work according to Ref. [21].

Here, the recovery stress of SMA wires is calculated based on the simplified form of the Brinson model in which the martensite volume fraction is separated into stress-induced ξ_s and temperature-induced components ξ_T. Based on the simplified Brinson model; the recovery stress can be calculated in the following form [22]:

$$\begin{aligned}
&\xi=\xi_s+\xi_T\\
&\sigma_r=E_s\left(\xi\right)\left(\varepsilon-\varepsilon_L\xi_s\right)+\Theta\Delta T
\end{aligned} \quad (3)$$

Where ε_L denotes the maximum residual strain, Θ is related to the CTE of SMAs, ΔT is temperature variations, and E_s refers to young's modulus of SMA wires expressed based on the Reuss model as:

$$E_s\left(\xi\right)=\frac{E_A}{1+\left(\frac{E_A}{E_M}-1\right)\xi} \quad (4)$$

In which, E_A and E_M are defined as young's modulus of the SMA in the pure austenite and pure martensite phases, respectively. According to Brinson martensite fractions during the heating stage can be calculated as:

$$\begin{aligned}
&\xi=\frac{\xi_0}{2}\left\{\cos\left[\frac{\pi}{A_f-A_s}\left(T-A_s-\frac{\sigma_r}{C_A}\right)\right]+1\right\}\\
&\xi_s=\xi_{s0}\frac{\xi}{\xi_0}.\quad \xi_T=\xi_{T0}\frac{\xi}{\xi_0}
\end{aligned} \quad (5)$$

Table 2. Material properties of the graphite fibers and graphite/epoxy composite [21]

Property	Value	
	graphite/epoxy composite	graphite fibers
Longitudinal Young modulus	129.62 GPa	213.13 GPa
Transverse Young modulus	7.23 GPa	23.11 GPa
Poisson ratio	0.27	0.2
Shear modulus	2.71 GPa	8.97 GPa
Transverse CTE	29.13×10^{-6} 1/^{0}C	-0.54×10^{-6} 1/^{0}C
Longitudinal CTE	0.18×10^{-6} 1/^{0}C	10.08×10^{-6} 1/^{0}C

Table 3. Material properties of 0.3 wt% CNT-reinforced epoxy polymer [23].

Property	Value
Young modulus	3.38 GPa
Poisson ratio	0.35
Glass transition temperature	110.5 ^{0}C
CTE	44×10^{-6} 1/^{0}C

Table 4. Material properties of nanocomposite (graphite/CNT/epoxy) [21]

Property	Value
Longitudinal Young modulus	129.74 GPa
Transverse Young modulus	7.71 GPa
Poisson ratio	0.27
Shear modulus	2.89 GPa
Transverse CTE	21.7×10^{-6} 1/^{0}C
Longitudinal CTE	-0.02×10^{-6} 1/^{0}C

where the subscript 0 represents the initial state of a parameter, since the martensite fraction depends on the stress and temperature, Eq. (3) must be coupled with Eq. (5) to formulate a complete governing equation for SMAs.

The Material properties of implemented SMA wires are [10] : $\rho=$ 6450 kg/m^3, α_s = 10.26×10^{-6} /^{0}C , ν =0.33 .Transformation temperatures: M_f =9 ^{0}C, M_s =18.4 ^{0}C, A_s =34.5 ^{0}C, A_f = 49 ^{0}C. Moduli: E_A =67GPa, E_M =26.3 GPa, Θ =0.55 MPa / ^{0}C . Phase diagram parameters: C_M =8 MPa / ^{0}C, C_A =13.8 MPa / ^{0}C, $(\sigma_s^{cr},\sigma_t^{cr})$ = (100,170) MPa.

In the present study, the role of adding 0.3 wt.% MWCNTs, in enhancing material properties of LY-5052 epoxy is investigated. Having some material properties of epoxy and CNT, it is possible to calculate the Young modulus of CNT-reinforced epoxy polymer with acceptable accuracy as follows [23]:

$$E_{NC}=\left[\frac{3}{8}\frac{1+2\left(l_{NT}/d_{NT}\right)\eta_L V_{NT}}{1-\eta_L V_{NT}}+\frac{5}{8}\frac{1+2\eta_L V_{NT}}{1-\eta_L V_{NT}}\right]E_P$$
$$\eta_L=\frac{\left(E_{NT}/E_p\right)-1}{\left(E_{NT}/E_p\right)+2\left(l_{NT}/d_{NT}\right)} \quad (6)$$
$$\eta_T=\frac{\left(E_{NT}/E_p\right)-1}{\left(E_{NT}/E_p\right)+2}$$

Where E_p and E_{NT} denote young's modulus of the epoxy and nanotubes, respectively. l_{NT}, d_{NT} and V_{NT} also represents the length, the outer diameter, and the volume fraction of MWCNTs.

Table 3 indicates the thermo-mechanical properties of the epoxy polymer reinforced by 0.3 wt% nanotubes.

Employing the rule of mixture, the material properties of graphite fiber/CNT/epoxy can be calculated, which are shown in Table 4.

2- 2- Equilibrium equations

The nonlinear strain-displacement relationship based on the von Karman assumption can be expressed as $\varepsilon_{xx}=\frac{\partial u}{\partial x}+\frac{1}{2}\left(\frac{\partial w}{\partial x}\right)^2-z\frac{\partial^2 w}{\partial x^2}$ [24]. The stress-strain relation for a *k*-th orthotropic lamina, which is subjected to the thermomechanical loadings, for an orthotropic laminated composite beam with arbitrary fiber orientation, can be written as $\sigma_x^k=\bar{Q}_{11}^k\left(\varepsilon_x^k-\alpha_x^k\Delta T\right)+cos^2\left(\theta^k\right)V_s{}^k\sigma_r^k$ where (T_0) is the reference temperature, ΔT is the temperature difference between current temperature (T) and θ^k the ply angle in the *k*-th layer. Furthermore, during the temperature rise σ_r^k show the effective recovery stress of SMA fibers. Also, α_x^k describes the thermal expansion coefficients [24].

The resultant force and moment for the SMA composite

laminate are defined as:

$$\begin{Bmatrix} N_{xx} \\ M_{xx} \end{Bmatrix} = \begin{bmatrix} A_{11} & B_{11} \\ B_{11} & D_{11} \end{bmatrix} \begin{Bmatrix} \dfrac{\partial u}{\partial x} + \dfrac{1}{2}\left(\dfrac{\partial w}{\partial x}\right)^2 \\ -\dfrac{\partial^2 w}{\partial x^2} \end{Bmatrix} - \begin{Bmatrix} N^T \\ M^T \end{Bmatrix} + \begin{Bmatrix} N^r \\ M^r \end{Bmatrix} \tag{7}$$

Which superscripts r refer to the in-plane forces and T refer to moments induced by SMA fibers and temperature rise, and can be written as

$$\begin{aligned} \left(N^r, M^r\right) &= \sum_{k=1}^{n} \int_{h_k-1}^{h_k} \sigma^r V_s cos^2\left(\theta^k\right)(1, z)\, dz \\ \left(N^T, M^T\right) &= \sum_{k=1}^{n} \int_{h_k-1}^{h_k} \left(\bar{Q}_{11}\alpha_x + \bar{Q}_{12}\alpha_y\right)^k \Delta T(1, z)\, dz \end{aligned} \tag{8}$$

Moreover, A_{11}, B_{11}, D_{11} are coupling and bending stiffness parameters and obtained as follows:

$$\left(A_{11}, B_{11}, D_{11}\right) = \sum_{k=1}^{n} \int_{h_k-1}^{h_k} \left(\bar{Q}_{11}\right)^k \left(1, z, z^2\right) dz \tag{9}$$

For hybrid laminated composite beams reinforced with SMA fibers, equations of motion may be obtained from Hamilton's principle. Based on Hamilton's principle, when the following condition in a structure is satisfied, an equilibrium position occurs:

$$\int_{t_1}^{t_2} \left(\delta U + \delta W - \delta K\right) dt = 0 \tag{10}$$

Where δU , δK and δW are the virtual strain energy, the virtual kinetic energy, and the virtual work due to the external work, respectively, and expressed as follow:

$$\begin{aligned} \delta U &= \iint \sigma_{xx} \delta\varepsilon_{xx} dV \\ \delta K &= \iint \rho\left(\dot{w}\delta\dot{w} + \dot{u}\delta\dot{u}\right) dV \\ \delta W &= \iint \Delta P \delta w dV \end{aligned} \tag{11}$$

Where ΔP is the aerodynamic load and can be written based on the supersonic piston theory which is a linear function of the lateral deflection. After some mathematical manipulations and integration by parts to eliminate the virtual displacements, the equations of motion are created as:

$$\begin{aligned} & I_0 \ddot{u} - I_1 \frac{\partial \ddot{w}}{\partial x} - \frac{\partial N_{xx}}{\partial x} = 0 \\ & I_0 \ddot{w} + \frac{\partial}{\partial x}\left(I_1 \ddot{u} - I_2 \frac{\partial \ddot{w}}{\partial x}\right) + \\ & \frac{\partial^2 M_{xx}}{\partial x^2} - N_{xx} \frac{\partial^2 w}{\partial x^2} + \Delta P = 0 \end{aligned} \tag{12}$$

where $I_i = \sum_{k=1}^{n} \int_{h_{k-1}}^{h_k} \rho^k z^i dz$ and ρ^k is the mass density of the constituent materials in the *k*-th layer. The simplified version of the nonlinear governing equation, by assuming in-plane and rotational inertia terms are negligible, is expressed as:

$$\begin{aligned} & \frac{\partial N_{xx}}{\partial x} = 0 \\ & I_0 \ddot{w} + \frac{\partial^2 M_{xx}}{\partial x^2} - N_{xx} \frac{\partial^2 w}{\partial x^2} + \Delta P = 0 \end{aligned} \tag{13}$$

The boundaries of the composite beam are assumed to be fully stationary in the in-plane direction, i.e., $u(0,t) = u(L,t) = 0$. From $\frac{\partial N_{xx}}{\partial x} = 0$ can be concluded that the axial load N_{xx} along the x axis is constant. According to the resultant force from Eq. (8) and integrating the above equation, yields $u(x,t) = -\frac{1}{2}\int_0^x \left(\frac{\partial w}{\partial x}\right)^2 dx + \frac{B_{11}}{A_{11}}\frac{\partial w}{\partial x} - \frac{x}{A_{11}}\left(N^T - N^r + C_1(t)\right) + C_2(t)$. At the fixed edges conditions, the parameters $C_1(t)$ and $C_2(t)$ can be obtained.

Finally, the nonlinear governing equation of motion of the hybrid laminated composite beam with embedded SMA fiber was developed as follows:

$$\begin{aligned} & I_0 \frac{\partial^2 w}{\partial t^2} + \left(D_{11} - \frac{B_{11}^2}{A_{11}}\right)\frac{\partial^4 w}{\partial x^4} + \\ & \left(N^T - N^r - \frac{A_{11}}{2L}\int_0^L \left(\frac{\partial w}{\partial x}\right)^2 dx\right)\frac{\partial^2 w}{\partial x^2} + \Delta P \\ & - \frac{B_{11}}{L}\left\{\frac{\partial w(L,t)}{\partial x} - \frac{\partial w(0,t)}{\partial x}\right\}\frac{\partial^2 w}{\partial x^2} = 0 \end{aligned} \tag{14}$$

Besides, based on the supersonic piston theory [25]:

$$\Delta P = -\zeta \frac{\partial w}{\partial x} - \varsigma \frac{\partial w}{\partial t}$$
$$\zeta = \frac{\rho_\infty u_\infty^2}{\sqrt{M_\infty^2 - 1}} \quad , \tag{15}$$
$$\varsigma = \frac{\rho_\infty u_\infty \left(M_\infty^2 - 1\right)}{\sqrt{\left(M_\infty^2 - 1\right)^3}}$$

Where ρ_∞ is free stream air density, u_∞ is velocity, and M_∞ is Mach number. As the aerodynamic damping term in Eq. (14) permanently balances the flutter boundary to examine the aerothermal characteristics of the supersonic beam using the SMA actuation, to develop the flutter equation of the beam, we can use the aerodynamic load without the aerodynamic damping.

$$I_0 \frac{\partial^2 w}{\partial t^2} + D_{11} \frac{\partial^4 w}{\partial x^4} + \left(N^T - N^r - \right. \tag{16}$$
$$\left. \frac{A_{11}}{2L} \int_0^L \left(\frac{\partial w}{\partial x} \right)^2 dx \right) \frac{\partial^2 w}{\partial x^2} - \zeta \frac{\partial w}{\partial x} - \varsigma \frac{\partial w}{\partial t} = 0$$

2- 3- Solution method and flutter analysis

In this section, the flutter velocity and critical buckling temperature of the laminated composite beam with embedded SMA fibers are calculated with the Galerkin procedure. To solve Eq. (16), In the Galerkin technique, a sum of some auxiliary functions is considered where each of them satisfies the boundary conditions. In this work, we use the Eigenfunctions of the vibrating Euler-Bernoulli beam as the admissible function of the Galerkin method. The acceptable function for the beam with two simply supported edges can be expressed as:

$$w(x,t) = e^{\Omega t} \sum_{i=0}^{N} W_i \sin\left(\frac{i\pi x}{L} \right) \tag{17}$$

Substituting Eq. (17) into the Eq. (16) and multiplying the results by $\sin\left(\frac{i\pi x}{L}\right)$ and integrating over the domain [0, L], the relation $([M]\Omega^2 + [K]_L + [K]_{NL} + \{F\}^T - \{F\}^T - \{F\}^{\Delta P})\{W\} = \{0\}$ is obtained where the eigenvalues $\Omega = \tau + i\omega$ are in general complex numbers, which τ is the measurement of the damping and ω is the Eigen frequency. By solving complex eigenvalues of the system, the natural frequencies and damping ratio of the system can be calculated using the final equation as:

$$\left| [M]\Omega^2 + [K]_L + [K]_{NL} + \{F\}^T - \{F\}^r - \{F\}^{\Delta P} \right| = 0 \tag{18}$$

It is obvious when flutter occurs, two successive Eigen frequencies of structures will unify at flutter velocity which is a specific flight velocity of the aircraft. As a result, if one would enhance the aerothermal flutter response of an aircraft structure, one should move towards the right of the coalescent point of the two Eigen frequencies or increase the flutter velocity.

Table 5. Comparison of frequency parameter $\Omega = \omega L \sqrt{\rho_m / E_m}$ **for the beam with** $L/h = 10$, $V_{cnt} = 0.12$

Model	Pattern of CNTs	
	UD	FG-X
Yas and Samadi [26]	1.2581	1.3859
Ki et al.[27]	1.2576	1.3852
Present	1.2580	1.3839

3- Numerical Results and Discussion

3- 1- Validation

Firstly, to validate the results of the analysis of the eigenvalues, the dimensionless natural frequency of beam reinforced with CNT at different reinforced phase patterns is presented in Table 5. The results show the high accuracy and precision of the present model.

In addition, to validate the results of stability diagrams in thermo-aerodynamic conditions, the results of the present analysis with the article of Samadpour et al. [11] for a symmetrical layer beam $[0/0/90]_s$ with shape memory alloy wires in two layers that are furthest from the center of the beam are compared for two different length-to-thickness ratios and are showed in Fig. 2 .The vertical axis of the diagram represents the dimensionless aerodynamic pressure parameter defined as [11]: $\lambda = \frac{1}{E_m^{ref}} \frac{\rho_\infty u_\infty^2}{\sqrt{M_\infty^2 - 1}} \left(\frac{L}{h}\right)^3$,(E_m^{ref} is the young modulus of the matrix at the reference temperature).

The results showed a good agreement between the present analysis and the reference article. According to Fig. 2, with increasing the L/h ratio of the beam, its flexural stiffness is reduced and we will see a smaller range of stability and a decrease in the maximum dimensionless aerodynamic

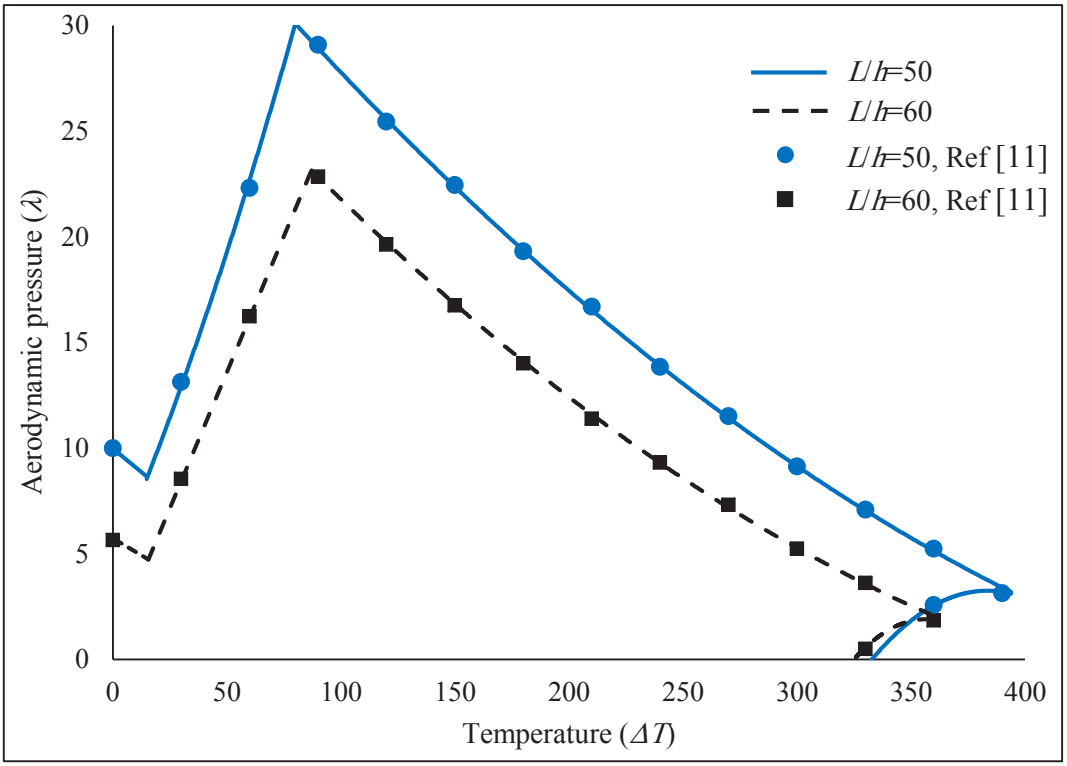

Fig. 2. Validation of aerothermodynamics stability diagrams of composite beams containing SMA wires, when $V_s = 10\%, \quad \varepsilon_0 = 1\%$

pressure .According to Fig. 2, the area of each curve can be divided into three areas. The first area is flat and is a balanced area in which the beam is not buckled or flattened. The second area is related to the buckling beam, which, of course, is still dynamically stable, in which the thermal load prevails over the beam stiffness and the aerodynamic stiffness. In addition, the beam suffers from static instability due to the thermal load. The third region is also dynamically unstable and has a fluttering phenomenon due to aerodynamic pressure.

3- 2- Parametric study of dynamic stability

The effect of SMA and CNT volume fractions on the stability curve of beam flutter under thermal field and aerodynamics load are demonstrated in Fig. 3.

According to Fig. 3, for a beam without CNT ($V_{cnt} = 0$), by doubling the memory alloy in the beam, the critical buckling temperature is approximately doubled because the presence of alloys has increased the bearing capacity of the axial beam load. Moreover, when $V_s = 10\%$, the maximum critical aerodynamic pressure for the CNT / SMA hybrid nanocomposite beam with $V_{cnt} = 0.14$ at $T = 385^{\circ}\mathrm{C}$ is almost doubled in the beam without CNT.

Fig. 4 illustrated stability curves of flutter nanocomposite beam reinforced with SMA wire and uniform distribution of CNT for different volume fractions of CNTs and prestressed SMA wires. According to Fig. 4, two entirely distinct turning points are seen in the stability curves of the beam, which have the maximum aerodynamic critical pressure and the maximum critical temperature. These two points almost correspond to the start temperature of the austenite phase and the end temperature of the intelligent material phase transition. Because the austenite phase completion temperature is a function of the amount of prestressing in the fibers, these points are varied for different curves.

As shown in Fig. 4, by doubling the pre-stress percentage, the maximum critical aerodynamic pressure of the beam at 100° C is increased by 70%. Changing the prestressing and the volume fraction of the shape memory alloy wires, the stability range is shifted to the right and higher temperatures because the critical buckling temperature has increased despite this memory alloy. Also, with increasing prestress and volume fraction of the alloys, the amount of dimensionless critical aerodynamic pressure has not changed much, because these alloys can increase the crucial pressure at specific temperatures. However, it is observed that the presence of carbon nanotubes has led to an increase in the maximum necessary aerodynamic pressure and their critical buckling temperature. On the other hand, as the volume fraction of

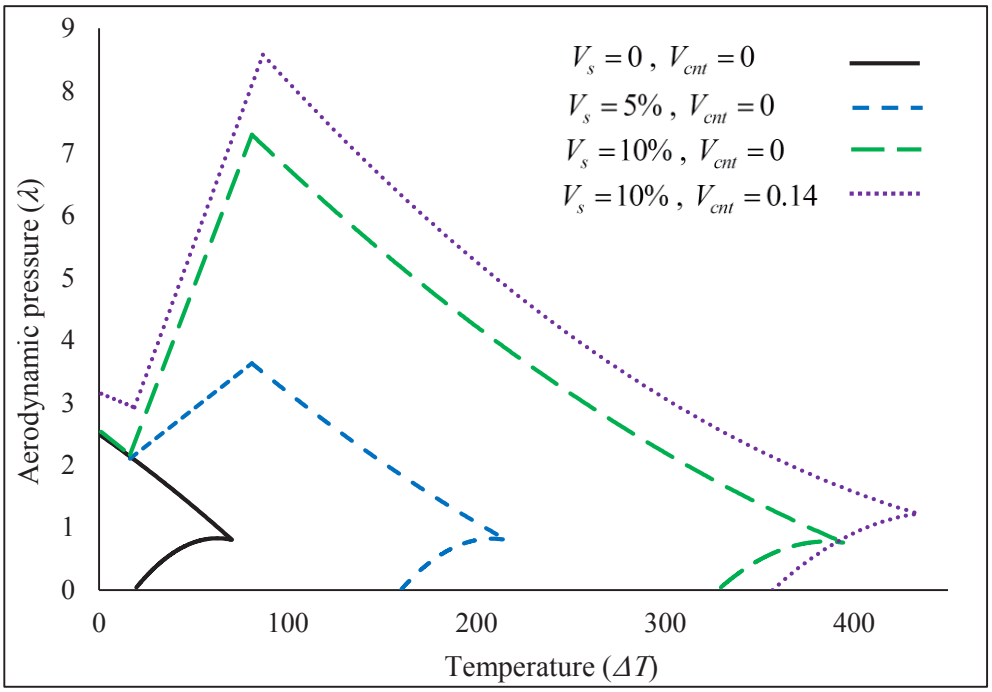

Fig. 3. Effect of SMA and CNT volume fractions on the stability curves of the beam ($L/h = 50$, $\varepsilon_0 = 1\%$)

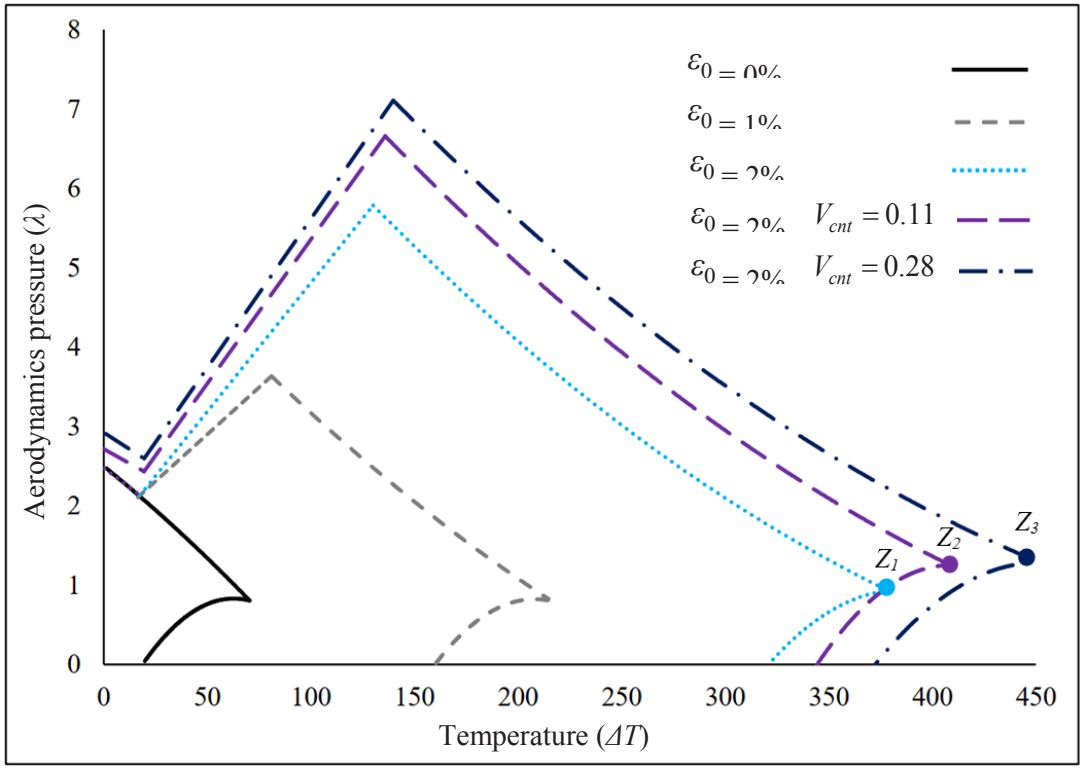

Fig. 4. Stability curves of flutter composite beam reinforced for different volume fractions of CNTs and ε_0 , for $L/h = 50$, $V_s = 5\%$.

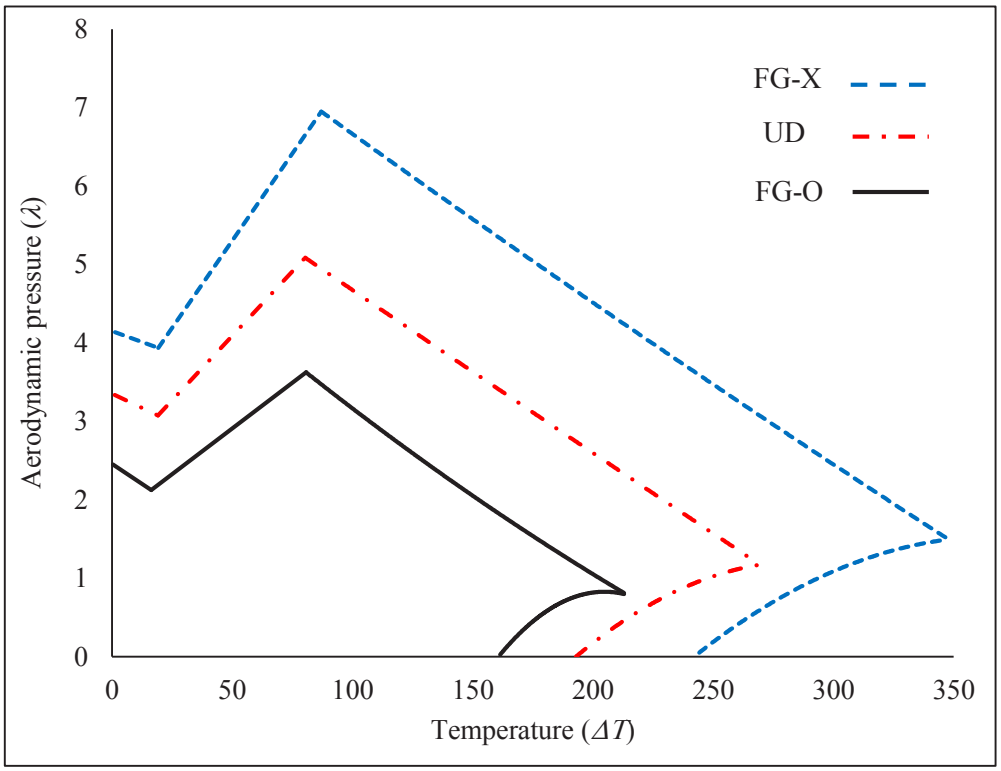

Fig. 5. Effect of CNT distribution in a hybrid composite beam containing CNT / SMA on its stability boundaries and aerothermodynamic flutter

the nanotubes in the beam increases, the points Z_1, Z_2, and Z_3 correspond to the existing curves to the right and up at higher temperatures and critical aerodynamic pressures.

Effects of CNT distribution on stability boundaries and aerothermodynamics of hybrid nanocomposite beam are plotted in Fig. 5. According to Fig. 5, the placement of nanotubes in the central layers of the composite and the FG-O arrangement has reduced the beam stability range relative to the uniform distribution of nanotubes in the layers (UD). On the other hand, their placement in the layers far from the center of the composite has increased the stability of the filter compared to the UD composite beam. Since the addition of nanotubes to each layer increases the effective modulus of that layer, so adding them to the composite intermediate layers and in the FG-O arrangement keeps the beam flexural stiffness to a minimum compared to the FG-X and UD distributions. For example, in nanocomposite beams containing CNT/SMA values and parameters $L/h=50$, $V_s=5\%$, $\varepsilon_0=1\%$ and $V_{cnt}=0.11$, the maximum critical aerodynamic pressure for the FG-X arrangement at $T=50^{\circ}\mathrm{C}$ is doubled and 1.4 times the value in FG-O and UD forms, respectively.

4- Conclusion

The main objective of the current study is to simultaneously examine the impact of carbon nanotubes and alloy memory wire on improving the behavior of composite beam flutter under the effect of ultrasonic flow and significant heat increase. Then the maximum critical aerodynamic pressure and maximum critical buckling temperature for this hybrid composite beam were calculated. The results showed that the simultaneous application of two advanced reinforcing materials has a remarkable influence on increasing the static and dynamic stability of laminated composite beams against the effects of thermal-aerodynamic loading. The most important results are:

By changing the prestress amount and the volume fraction of the memory alloys, the stability range is shifted to the right and higher temperatures because the critical buckling temperature has increased despite this memory alloy.

As the volume fraction of nanotubes in the beam increases, the range of the stability curve increases towards higher temperatures and critical aerodynamic pressures.

The placement of nanotubes in the interlayer layers of the composite and the FG-O arrangement has reduced the beam stability range relative to the uniform distribution

of nanotubes in the layers (UD). On the other hand, their placement in layers away from the center of the composite has increased the flutter compared to the UD composite beam.

By doubling the pre-stress percentage, the maximum critical aerodynamic pressure of the beam at $100\,^{\circ}\mathrm{C}$ is increased by 70%.

when $V_s = 10\%$, the max. critical aerodynamic pressure for the CNT / SMA hybrid nanocomposite beam with $V_{cnt} = 0.14$ at $T = 385\,^{\circ}\mathrm{C}$ is doubled in the beam without CNT.

For the CNT / SMA hybrid nanocomposite beam, the max. critical aerodynamic pressure for the FG-X arrangement at $T = 50\,^{\circ}\mathrm{C}$ is doubled and 1.4 times the value in FG-O and UD forms, respectively.

References

[1] D.C. Lagoudas, Shape memory alloys: modeling and engineering applications, Springer Science & Business Media, (2008).

[2] Z.C. Feng, D.Z. Li, Dynamics of a mechanical system with a shape memory alloy bar, Journal of Intelligent Materials Systems and Structures, 7 (4) (1996) 399-410.

[3] D. Bernardini, G. Rega, Thermomechanical modelling, nonlinear dynamics and chaos in shape memory oscillators, Mathematical and Computer Modelling of Dynamical Systems, 11 (3) (2005) 291-314.

[4] M.A. Savi, P. Pacheco, Chaos and hyperchaos in shape memory systems, International Journal of Bifurcation and Chaos, 12 (3) (2002) 645-657.

[5] L.G. Machado, M.A. Savi, P.M. Pacheco, Nonlinear dynamics and chaos in coupled shape memory oscillators, International Journal of Solids and Structures, 40 (19) (2003) 5139-5156.

[6] D. Lagoudas, L. Machado, M. Lagoudas, Nonlinear vibration of a one-degree of freedom shape memory alloy oscillator: a numerical-experimental investigation, In 46th AIAA/ASME/ASCE /ASC Structures, Structural Dynamics and Materials Conference, (2005) 2119.

[7] X.Y. Tsai, L.W. Chen, Dynamic stability of a shape memory alloy wire reinforced composite beam, Composite Structures, 56 (3) (2002) 235-241.

[8] S.M.R. Khalili, M.B. Dehkordi, E. Carrera, A nonlinear finite element model using a unified formulation for dynamic analysis of multilayer composite plate embedded with SMA wires, Composite Structures, 106 (2013) 635-645.

[9] S.M.T. Hashemi, S.E. Khadem, Modeling and analysis of the vibration behavior of a shape memory alloy beam, International Journal of Mechanical Sciences, 48 (1) (2006) 44-52.

[10] A.R. Damanpack, M. Bodaghi, M.M. Aghdam, M. Shakeri, On the vibration control capability of shape memory alloy composite beams, Composite Structures, 110 (2014) 325-334.

[11] M. Samadpour, H. Asadi, Q. Wang, Nonlinear aero-thermal flutter postponement of supersonic laminated composite beams with shape memory alloys, European Journal of Mechanics, 57 (2016) 18-28.

[12] H. Asadi, A.R. Beheshti, On the nonlinear dynamic responses of FG-CNTRC beams exposed to aerothermal loads using third-order piston theory, Acta Mechanica, 229 (6) (2018) 2413-2430.

[13] H. Lin, C. Shao, D. Cao, Nonlinear flutter and random response of composite panel embedded in shape memory alloy in thermal-aero-acoustic coupled field, Aerospace Science and Technology, 100 (2020) 105785.

[14] A. Rostamijavanani, M.R. Ebrahimi, S. Jahedi, Thermal post-buckling analysis of laminated composite plates embedded with shape memory alloy fibers using semi-analytical finite strip method, Journal of Failure Analysis and Prevention, 21 (1) (2021) 290-301.

[15] A. Kumar, K. Sharma, A.R. Dixit, Carbon nanotube-and graphene-reinforced multiphase polymeric composites: review on their properties and applications, Journal of Materials Science, 55 (7) (2020) 2682-2724.

[16] M.F.L. De Volder, S.H. Tawfick, R.H. Baughman, A.J. Hart, Carbon nanotubes: present and future commercial applications, Science, 339 (6119) (2013) 535-539.

[17] C. Wang, Y. Xu, J. Du, Study on the thermal buckling and post-buckling of metallic sub-stiffening structure and its optimization, Materials and Structures, 49 (11) (2016) 4867-4879.

[18] K. Mehar, P.K. Mishra, S.K. Panda, Numerical investigation of thermal frequency responses of graded hybrid smart nanocomposite (CNT-SMA-Epoxy) structure, Mechanics of Advanced Materials and Structures, 1 (2020) 1–13.

[19] K. Mehar, P.K. Mishra, S.K. Panda, Thermal buckling strength of smart nanotube-reinforced doubly curved hybrid composite panels, Computers & Mathematics with Applications, 90 (2021) 13-24.

[20] S. Kamarian, M. Bodaghi, R.B. Isfahani, M. Shakeri, M.H. Yas, Influence of carbon nanotubes on thermal expansion coefficient and thermal buckling of polymer composite plates: Experimental and numerical investigations, Mechanics Based Design of Structures and Machines, 49 (2) (2021) 217-232.

[21] S. Kamarian, M. Bodaghi, R.B. Isfahani, J. Song, A comparison between the effects of shape memory alloys and carbon nanotubes on the thermal buckling of laminated composite beams, Mechanics Based Design of Structures and Machines, 1 (2020) 1-24.

[22] L.C. Brinson, M.S. Huang, Simplifications and comparisons of shape memory alloy constitutive models, Journal of Intelligent Materials Systems and Structures, 7 (1) (1996) 108-114.

[23] D. Qian, E.C. Dickey, R. Andrews, T. Rantell, Load transfer and deformation mechanisms in carbon nanotube-polystyrene composites, Applied Physics Letters, 76 (20) (2000) 2868-2870.

[24] J.N. Reddy, Mechanics of laminated composite plates and shells: theory and analysis, CRC press, (2003).

[25] R.L. Bisplinghoff, H. Ashley, Principles of aeroelasticity. Courier Corporation, (2013).

[26] M.H. Yas, N. Samadi, Free vibrations and buckling

analysis of carbon nanotube-reinforced composite Timoshenko beams on elastic foundation, International Journal of Pressure Vessels and Piping, 98 (2012) 119-128.

[27] L.L. Ke, J. Yang, S. Kitipornchai, Nonlinear free vibration of functionally graded carbon nanotube-reinforced composite beams, Composite Structures, 92 (3) (2010) 676-683.

HOW TO CITE THIS ARTICLE

H. Heidari, S. Esmaeili, A. Hakimi, Effects of Shape Memory Alloys and Carbon Nanotubes on the Nonlinear Aerothermal Flutter Characteristics of Hybrid Nanocomposite Beam, AUT J. Mech Eng., 6(2) (2022) 217-228.

DOI: 10.22060/ajme.2022.20395.6000